AIAA 97-3812
Entry Dispersion Analysis for the Stardust Comet Sample Return Capsule

Prasun N. Desai
Robert A. Mitcheltree
F. McNeil Cheatwood
NASA Langley Research Center
Hampton, VA

1997 AIAA
GNC, AFM, and MST
Conference and Exhibit
August 11-13, 1997
New Orleans, LA

ENTRY DISPERSION ANALYSIS FOR THE STARDUST COMET SAMPLE RETURN CAPSULE

Prasun N. Desai*
Robert A. Mitcheltree†
F. McNeil Cheatwood‡
NASA Langley Research Center
Hampton, VA 23681-0001

ABSTRACT

Stardust will be the first mission to return samples from beyond the Earth-Moon system. The sample return capsule, which is passively controlled during the fastest Earth entry ever, will land by parachute in Utah. The present study analyzes the entry, descent, and landing of the returning sample capsule. The effects of two aerodynamic instabilities are revealed (one in the high altitude free molecular regime and the other in the transonic/subsonic flow regime). These instabilities could lead to unacceptably large excursions in the angle-of-attack near peak heating and main parachute deployment, respectively. To reduce the excursions resulting from the high altitude instability, the entry spin rate of the capsule is increased. To stabilize the excursions from the transonic/subsonic instability, a drogue chute with deployment triggered by an accelerometer and timer is added prior to main parachute deployment. A Monte Carlo dispersion analysis of the modified entry (from which the impact of off-nominal conditions during the entry is ascertained) shows that the capsule attitude excursions near peak heating and drogue chute deployment are within Stardust program limits. Additionally, the size of the resulting 3-σ landing ellipse is 83.5 km in downrange by 29.2 km in crossrange, which is within the Utah Test and Training Range boundaries.

NOMENCLATURE

CFD	Computational Fluid Dynamics
c.g.	Center-of-Gravity
DOF	Degree-of-Freedom
DSMC	Direct Simulation Monte Carlo
LAURA	Langley Aerothermodynamic Upwind Relaxation Algorithm
NASA	National Aeronautics and Space Administration
NNE	North-Northeast
PICA	Phenolic Impregnated Carbon Ablator
POST	Program to Optimize Simulated Trajectories
SRC	Sample Return Capsule
SSW	South-Southwest
TLNS3D	Thin Layer Navier Stokes Three-Dimensional
UTTR	Utah Test and Training Range
α_T	Total angle-of-attack (angle between the spin axis and velocity vector), deg
γ	Flight-path angle, deg

INTRODUCTION

The fourth of NASA's Discovery class missions is a comet sample return mission known as Stardust. It will be the first mission to return samples from beyond the Earth-Moon system. The spacecraft is scheduled to be launched in February of 1999 for encounter with the comet Wild-2 in 2004. Stardust will come within 100 km of the comet nucleus and deploy a sample tray to collect cometary and interstellar dust particles (Fig. 1a). Upon Earth return in January 2006, the entry capsule (Fig. 1b), containing the comet samples, will be released from the spacecraft and land by parachute at the Utah Test and Training Range (UTTR). The entry velocity will be the highest of any Earth-returning mission (relative velocity

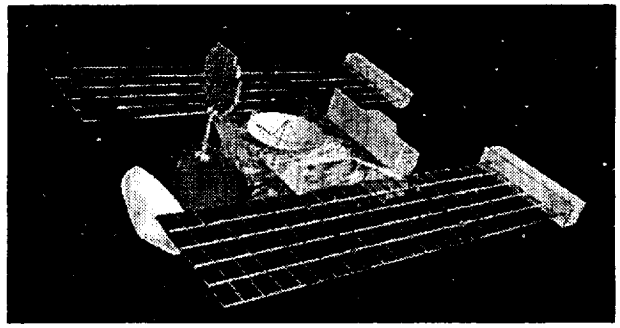

Fig. 1a. Stardust spacecraft flight configuration.

*Aerospace Engineer, Vehicle Analysis Branch, Space Systems and Concepts Division, Senior Member AIAA.
†Aerospace Engineer, Aerothermodynamics Branch, Aero and Gas-Dynamics Division, Senior Member AIAA.
‡Aerospace Engineer, Vehicle Analysis Branch, Space Systems and Concepts Division, Member AIAA.

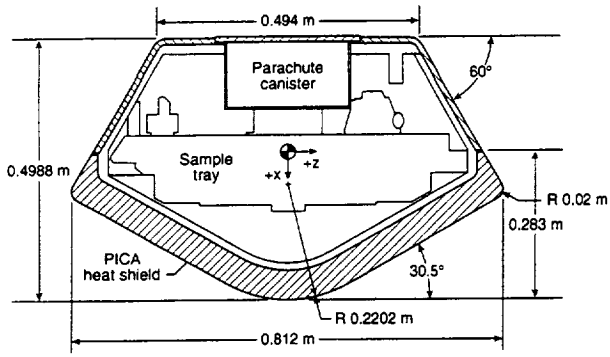

Fig. 1b. Stardust sample return capsule configuration.

about 12.6 km/s). A new heat shield made of PICA (Phenolic Impregnated Carbon Ablator) will be used to protect the Sample Return Capsule (SRC) from the intense heat of reentry.[1]

Four hours prior to entry, the SRC will be spun-up and separated from the main bus. The SRC has no active control system, so the spin-up is required to maintain its entry attitude (nominal 0° angle-of-attack) during coast. Throughout the atmospheric entry, the passive SRC will rely solely on aerodynamic stability for performing a controlled descent through all aerodynamic flight regimes: hypersonic-rarefied, hypersonic-transitional, hypersonic-continuum, supersonic, transonic, and subsonic. The SRC must possess sufficient aerodynamic stability to overcome the gyroscopic (spin) stability in order to minimize any angle-of-attack excursions during the severe heating environment. Additionally, this stability must persist through the transonic and subsonic regimes to maintain a controlled attitude at parachute deployment.

The objective of this study is to analyze the entry, descent, and landing of the returning sample capsule. This analysis consists of performing a trajectory simulation of the entire entry (from bus separation to landing) to predict the descent attitude and landing conditions. In addition, a Monte Carlo dispersion analysis is performed to ascertain the impact of off-nominal conditions which may arise during the entry to determine the robustness of the Stardust SRC design. Specifically, the SRC attitude near peak heating and parachute deployment is of interest, along with the landing footprint ellipse.

The SRC is restricted to land within the UTTR site. For mission success, a high-fidelity aerodynamic database is essential in order to accurately predict the landing location, as well as the attitude of the SRC at critical phases (e.g., peak heating and parachute deployment) during the entry. In this paper, the aerodynamics utilized in the entry simulation is mentioned first, followed by a description of the nominal entry sequence of the SRC. Finally, the results of the Monte Carlo entry dispersion analysis are presented.

ANALYSIS

Aerodynamics

The aerodynamic database utilized for the SRC in the flight simulation studies is constructed from a combination of computational fluid dynamics (CFD) calculations, and wind tunnel and historical flight data as described by Mitcheltree, et. al.[2] This large variety of sources for the aerodynamics is required because the SRC traverses many different flow regimes (hypersonic-rarefied, hypersonic-transitional, hypersonic-continuum, supersonic, transonic, and subsonic) during its entry. At the outer reaches of the atmosphere, free molecular flow aerodynamics are employed. In the rarefied flow regime, Direct Simulation Monte Carlo (DSMC) simulations up to angles-of-attack of 30 degrees are used to define bridging functions for the aerodynamic coefficients. In the hypersonic-continuum regime, a matrix of 22 solutions from the computational fluid dynamics code LAURA (Langley Aerothermodynamic Upwind Relaxation Algorithm)[3] describe the aerodynamics for Mach numbers between 42 and 7.15. At supersonic and transonic speeds, the aerodynamics are taken from two sets of existing wind tunnel data, augmented by CFD results from the TLNS3D (Thin Layer Navier Stokes Three-Dimensional) code.[4] Subsonic aerodynamics are defined by a combination of static wind tunnel measurements and dynamic free flight measurements.[5] These sources are blended to form a comprehensive database which describes the aerodynamics of the SRC for the expected flight conditions. Figure 2 shows the range of application of the various aerodynamic sources mentioned above. The aerodynamic characteristics of the SRC are described in detail in Ref. 2.

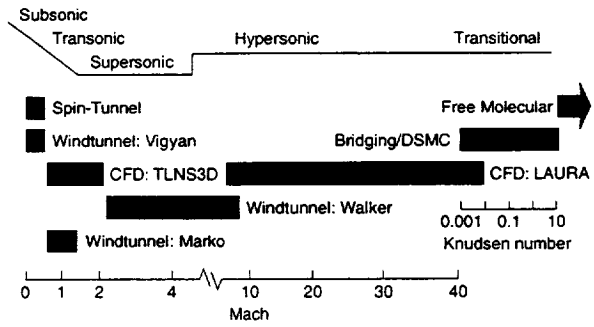

Fig. 2 Stardust SRC aerodynamic database.

Trajectory Simulation

The trajectory analysis is performed using the six- and three-DOF (degree-of-freedom) versions of the Program to Optimize Simulated Trajectories (POST).[6] This program has been utilized previously for similar applications.[7,8,9] The three-DOF program (which integrates the translation equations of motion) is used from bus separation to atmospheric interface. The six-DOF version of POST (which integrates the translational and rotational equations of motion) is used from atmospheric interface until parachute deployment. The three-DOF program is used again from parachute deployment to landing. The trajectory simulation includes Earth atmospheric (GRAM-95)[10] and gravitational models, capsule separation and non-instantaneous parachute deployment models, and capsule aerodynamics and mass properties. The validity of the present approach has been demonstrated recently through comparisons between the Mars Pathfinder pre-flight predictions of the flight dynamics and the flight data.[11]

During the entry, off-nominal conditions may arise which affect the descent profile. These off-nominal conditions can originate from numerous sources, such as capsule mass property measurement uncertainties, separation attitude and attitude rate uncertainties, and limited knowledge of the flight-day atmospheric properties (density, pressure, and winds). Additionally, computational uncertainty with the aerodynamic analysis and uncertainties with parachute deployment are contributing sources of uncertainty. In this analysis, an attempt is made to conservatively quantify and model the degree of uncertainty in each mission parameter. For this mission, 41 potential uncertainties were identified. These uncertainties are grouped into two categories (exo-atmospheric and atmospheric) and are listed in Tables 1 and 2, respectively, along with the corresponding 3-σ variances. For most of the parameters, a Gaussian distribution is sampled. However, for the center-of-gravity (c.g.) offset quadrant and parachute deployment parameters (g-switch, timers, and aerodynamics), uniform distributions are utilized to model their operating performance.

As will be shown in the results, the successful return of the cometary samples by the Stardust SRC depends heavily on the validity of the Monte Carlo analysis more than any previous mission. Increased reliance on entry simulations for mission success places considerable importance on selecting appropriate uncertainties. As confidence increases in the analysis accuracy, cheaper and/or higher performance entry systems can be selected for future missions.

Table 1. Exo-Atmospheric Mission Uncertainties.

Mass Properties	**3-σ Variance**
Mass	±0.5 kg
cg position along spin axis	±0.254 cm
cg position off spin axis	±0.254 cm
Major moment of inertia (I_{xx}, I_{yy}, I_{zz})	±20%
Cross products of inertia (I_{xy}, I_{xz}, I_{yz})	±0.015 kg-m^2
Post-Separation State Vector	
Position, Velocity (correlated with coveriance matrix corresponding to $\Delta\gamma_f$)	±0.075 deg
Pitch attitude	±2.0 deg
Yaw rate	±6.0 deg/s
Roll rate	+4 rpm, −2 rpm
Separation	
Spring induced velocity:	
radial velocity	±0.0482 m/s
cross-track velocity	±0.0482 m/s
in-track velocity	±0.04 m/s

Table 2. Atmospheric Mission Uncertainties

Aerodynamic		**3-σ Variance**
Free molecular aerodynamics,	CA	±10%
	CN, CY	±8%
	Cm, Cw	±12%
Hypersonic continuum aerodynamics,	CA	±4%
	CN, CY	±8%
	Cm, Cw	±10%
Supersonic continuum aerodynamics,	CA	±10%
	CN, CY	±5%
	Cm, Cw	±8%
Subsonic continuum aerodynamics,	CA	±5%
Hypersonic dynamic stability coefficients,	Cmq, Cnr	±0.15
Supersonic dynamic stability coefficients,	Cmq, Cnr	±0.15
Atmosphere		
Pressure, density, winds: GRAM-95 model		3-σ scale factor
Other		
Ablation mass		±10%
* Drogue chute g-switch		±10%
* Drogue chute deployment timer		±1%
* Drogue chute aerodynamics,	CA	±10%
* Main chute deployment timer		±1%
* Main chute aerodynamics,	CA	±15%

*Uncertainty sampled using uniform distribution

RESULTS AND DISCUSSION

Nominal Mission

Original Entry Sequence

In the original nominal Stardust entry sequence, the SRC enters the atmosphere with a spin rate of 5 revolutions per minute (rpm). The spin rate maintains entry attitude (nominal 0° angle-of-attack) until atmospheric interface (since the SRC possesses no active control system). As the SRC descends, it must rely solely on atmospheric stability in all flow regimes to minimize any angle-of-attack excursions until main parachute deployment at Mach 0.16. However, the SRC was found to be statically unstable in the free molecular flow regime due to its aft center-of-gravity location (0.283 m or 0.351 body diameters back from the nose).[2] The six-DOF analysis reveals that the pitch rate induced by the instability during the free molecular regime carries into the transitional region where high angles-of-attack are produced. This static instability causes the SRC to pitch-up to a total angle-of-attack (α_T) above 70 deg as seen in Fig. 3. As the SRC descends into the continuum regime (where it is statically stable) the angle-of-attack damps out and reduces to small values.

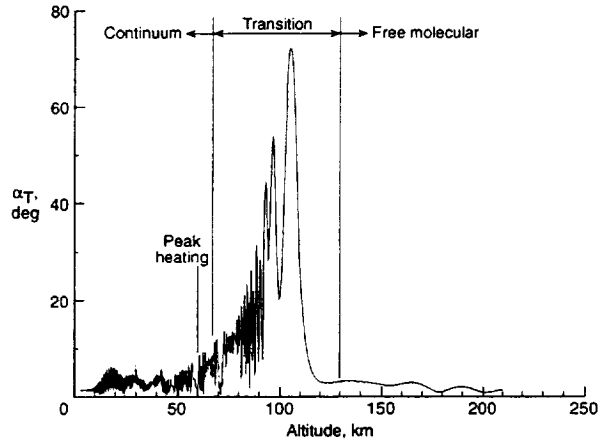

Fig. 3. Original nominal Stardust attitude profile.

High angles-of-attack early in the entry are a concern, since they can lead to angles-of-attack greater than 10 deg at peak heating (which is a Stardust program limit). Angles-of-attack greater than 10 deg increase afterbody heating near the shoulder regions and can damage the afterbody thermal protection system. Moreover, high angles-of-attack are worrisome because the SRC is stable flying backwards. Off-nominal attitude and attitude rate conditions at atmospheric interface could result in a backward entry. In addition to the high altitude static instability, a low altitude dynamic instability in the transonic and subsonic flow regimes also exists, again caused by the aft center-of-gravity location. This transonic/subsonic dynamic instability could induce a tumbling motion prior to main parachute deployment, raising concerns for a successful deployment. Reference 2 describes the SRC's stability/instability in the various regimes in more detail.

Modified Entry Sequence

The original nominal entry sequence is unacceptable since off-nominal conditions could result in mission failure. Modification of either the entry sequence or the SRC is required to improve the probability of mission success.

The high altitude and transonic/subsonic instabilities could be eliminated by moving the c.g. of the SRC forward to 0.26 body diameters back from the nose.[2] Since the SRC has only three major components (forebody heat shield, sample tray, and parachute canister), movement of the c.g. via re-packaging of the SRC is difficult. The size and mass of the sample tray preclude large movements in the c.g. Ballast could be added to the nose of the SRC to move the c.g. forward. However, a prohibitive large amount (22.4 kg) of ballast is required to move the c.g. sufficiently forward to remove the instabilities.

Augmentation of the SRC's stability is deemed necessary to eliminate the large angle-of-attack excursions. Several concepts were considered. For example, adding an aft-skirt would provide a restoring torque in the free-molecular regime stabilizing the SRC.[12] However, these devices, once serving their purpose, must be discarded in order to avoid destabilizing the lower flight regimes. To avoid such complications, the solution selected to address the high altitude instability is to increase the spin rate of the SRC upon entry. The higher spin rate, although not eliminating the instability, increases the gyroscopic stability of the SRC sufficiently to retard the effects of the free molecular static instability. However, if the entry spin rate is too large, the gyroscopic stability could overwhelm the aerodynamic stability in the continuum regime. This would lead to large angles-of-attack during peak heating. After a detailed investigation performing numerous six-DOF entry analyses for a variety of spin rates, an entry spin rate of 16 rpm is selected. This spin rate adequately reduces the high altitude angle-of-attack excursions, yet avoids any attitude concerns during peak heating. Additionally, a 16 rpm spin rate affords sufficient margin (in the angle-of-attack excursions) to accommodate off-nominal conditions which may be present during the entry (as confirmed by the Monte Carlo analysis presented later).

The transonic/subsonic instability is addressed by deploying a supersonic drogue chute prior to main parachute deployment. The drogue chute serves as a stabilizing mechanism for the SRC until main parachute deployment. The drogue chute size and deployment Mach number are constrained by the need to prevent excessive drift, which could lead to a landing footprint beyond the proposed UTTR site. However, the drogue chute size must provide sufficient area to stabilize the SRC. Furthermore, the deployment Mach number must be outside the dynamic instability region near transonic speeds to avoid the possibility of large angles-of-attack. From spin tunnel tests, the drogue chute is sized to 0.828 m in diameter to provide ample area for stabilizing the SRC.[5] Numerous six- and three-DOF analyses of the entry reveal that drogue deployment at Mach 1.4 avoids excessive drift concerns (as confirmed by the Monte Carlo results presented later).

Adoption of these changes into the mission required modification of the entire terminal descent procedure of the entry. A new deployment algorithm, consisting of a g-switch and two timers, is utilized for deployment of the drogue and main parachutes. Previously, only a baro-switch was needed for deploying the main parachute (diameter = 8.2 m). Figure 4 shows the modified nominal entry profile, with the terminal descent sequence highlighted. The g-switch is triggered after sensing 3 g's (decelerating side) for 0.5 seconds, at which point, the drogue timer is initiated. After 15.04 seconds, the drogue chute is deployed, initiating the main timer. After 350.6 seconds, the main parachute is deployed. This new nominal entry sequence is sufficiently robust to accommodate off-nominal conditions during the entry (as confirmed by the Monte Carlo analysis presented below).

Trajectory calculations are repeated for the modified entry profile using the most current mass properties

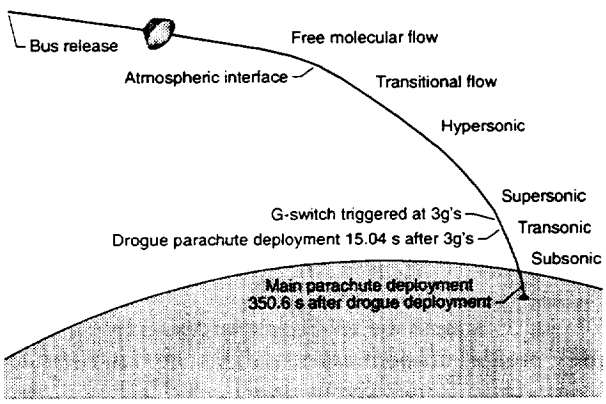

Fig. 4. Modified nominal Stardust entry sequence.

Table 3. Nominal Mass Properties of the SRC.

Mass, kg	46.0
Center of gravity, m	
Along spin axis (x-direction, from nose)	0.2831
Off spin axis (y-direction)	0.000396
Off spin axis (z-direction)	-0.002715
I_{xx}, kg-m^2 (spin axis)	2.163
I_{yy}, kg-m^2	1.595
I_{zz}, kg-m^2	1.4991
I_{xy}, kg-m^2	0.00181
I_{xz}, kg-m^2	0.00221
I_{yz}, kg-m^2	0.00437

for the SRC (Table 3). The flight characteristics of the modified nominal are shown in Figs. 5 and 6. During the entry, the SRC aerodynamically decelerates from 12.6 km/s to subsonic speeds. The maximum deceleration experienced by the SRC during the descent is 32.9 g's.

Recall that the SRC is still statically unstable in the free molecular regime. The higher spin rate only delays the effect of the static instability so that the SRC can traverse the transitional regime to the stable continuum regime without experiencing a large increase in the total angle-of-attack. As seen in Fig. 5, the total angle-of-attack pitches up to approximately 7 deg in the transitional regime before reducing to less than 2 deg near peak heating (which occurs around Mach 35.3). Reference 13 describes the heating environment encountered during the entry.

As the SRC descends, the static margin decreases near Mach 12 to produce a new trim point. Consequently, since the SRC has a non-zero c.g. off-set from the

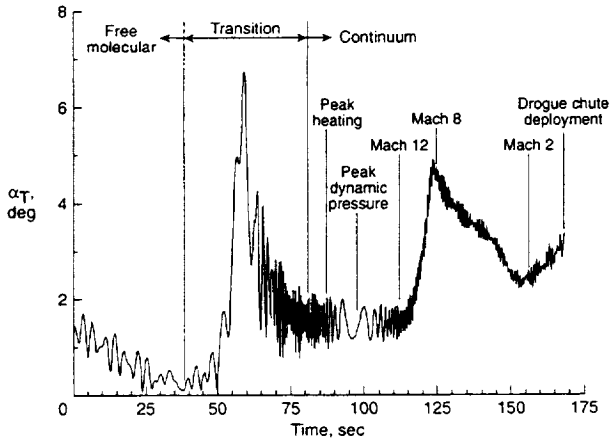

Fig. 5. Modified nominal Stardust attitude profile.

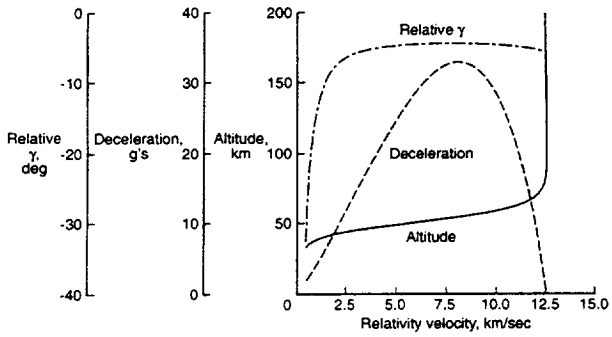

(a) Entry sequence.

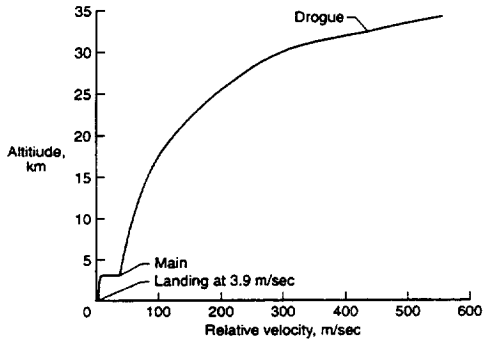

(b) Parachute deployment sequence.

Fig. 6. Modified nominal mission profile.

spin axis, an increase in α_T is observed from a mean α_T of approximately 1.5 deg near Mach 12 to approximately a mean α_T of 2.5 deg near Mach 2. In transitioning to a new trim point, attitude rates induce an overshoot in α_T (peaking around Mach 8) before receding around Mach 2. As the SRC approaches transonic speeds, the dynamic instability drives another increase in α_T until drogue chute deployment.

Beginning at Mach 1.4 (approximately 34 km altitude), the terminal descent phase of the entry begins, which slows the SRC down to approximately 4 m/s prior to landing. Figure 6b shows the nominal altitudes of the drogue and main parachute deployments.

Note, the mass properties for the SRC continue to fluctuate as its design matures. However, the current properties listed in Table 3 are representative of the final configuration.

Monte Carlo Dispersion Analysis

Independent Uncertainty Effects

Before a combination of off-nominal conditions are examined, a sensitivity analysis is first performed to identify the mission uncertainties which have the greatest impact on the overall landing footprint. Each of the 41 mission uncertainties are varied independently at their respective ±3-σ (maximum/minimum) variance. Figure 7 shows the resulting downrange obtained from the largest contributors to the overall landing footprint. Those mission uncertainties which are not depicted lead to downrange dispersions less than 0.5 km.

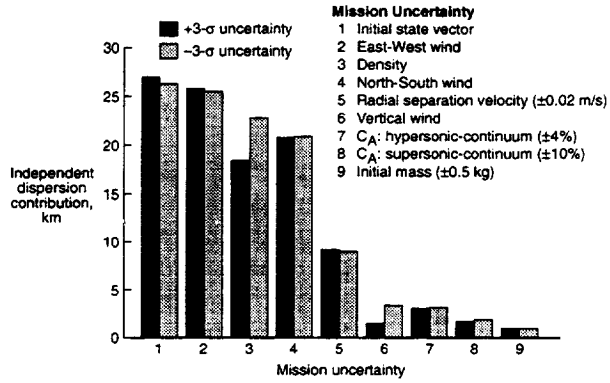

Fig. 7. Significant contributors to the total range dispersion. (3-σ variance shown in parenthesis.)

The mission uncertainties shown in Fig. 7 can be grouped into two categories: large contributors (mission uncertainties 1-4) and small contributors (mission uncertainties 5-9). The first group, containing initial state vector and atmospheric wind and density uncertainties, contribute on the order of 20-25 km each to the landing footprint size. Again, since the atmospheric winds have a significant impact on the downrange due to parachute drift, the selection of an appropriate drogue chute size and deployment Mach number is critical. The second group, containing uncertainties in initial mass, bus separation velocity, and aerodynamic drag, produce downrange dispersions of approximately 1-10 km each. Table 4 summarizes the independent ±3-σ dispersion results. Note that uncertainties in the aerodynamics associated with the mission have a minimal impact on the overall landing footprint.

Multiple Uncertainty Effects

To determine the robustness of the Stardust SRC entry profile, off-nominal conditions are simulated to address uncertainties which may arise during the descent. The impact of multiple uncertainties occurring simultaneously is ascertained by performing a Monte Carlo dis-

*Table 4. Major Contributors to Total Downrange Dispersion**

	Dispersion with +3-σ uncertainty, km	Dispersion with -3-σ uncertainty, km
1. State vector	26.9	26.2
2. East-West wind	25.8	25.5
3. Density	18.4	22.8
4. North-South wind	20.8	20.9
5. Radial separation velocity (±0.02 m/s)	9.2	9.0
6. Vertical wind	1.5	3.4
7. C_A: hypersonic-continuum (±4%)	3.1	3.2
8. C_A: supersonic-continuum (±10%)	1.7	1.9
9. Initial mass (±0.5 kg)	1.0	1.0

All other contributors < 0.5 km

*3-σ variance shown in parentheses

persion analysis. Over 3200 random trajectories are simulated to assure proper Gaussian or uniform distributions for the 41 mission uncertainties identified.

The statistical results from the 3200 Monte Carlo simulations are displayed in Figs. 8-15. Figures 8-10 show the distribution of the total angle-of-attack at three discrete locations during the early phase of the mission: at atmospheric interface, in the transitional regime, and at peak heating. At atmospheric interface, the statistical mean total angle-of-attack of the 3200 Monte Carlo cases is 2.5 deg. The maximum α_T observed is around 8 deg (which is below the mission constraint of 10 deg). In the transitional regime, the total angle-of-attack does increase from atmospheric interface due to the free molecular instability. The mean α_T is 8.1 deg, and the maximum α_T observed is 30.4 deg. The higher spin rate prevents continued growth in the total angle-of-attack; so that, by peak heating (where the SRC is stable), the mean α_T damps to 2.5 deg as seen in Fig. 10. The maximum α_T observed at peak heating is 8.6 deg, which is below the mission constraint of 10°.

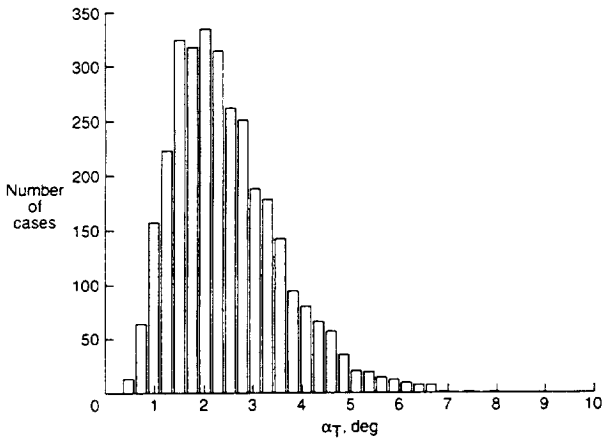

Fig. 8. Distribution of total angle-of-attack at atmospheric interface resulting from over 3200 Monte Carlo simulation cases.

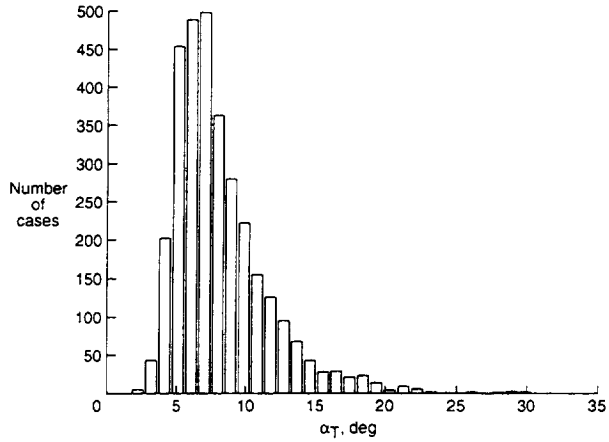

Fig. 9. Distribution of total angle-of-attack in transitional regime resulting from over 3200 Monte Carlo simulation cases.

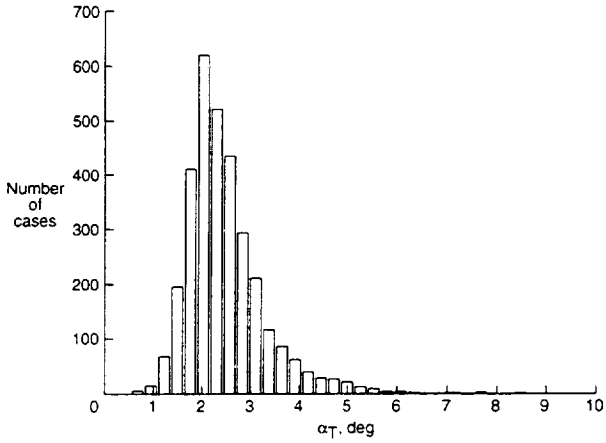

Fig. 10. Distribution of total angle-of-attack at peak heating resulting from over 3200 Monte Carlo simulation cases.

Figures 11-13 show the distribution of the drogue and main parachute deployment conditions. The mean Mach number at drogue chute deployment is 1.4, as seen in Fig. 11. The minimum deployment Mach number encountered is 1.27, which is high enough to avoid the significant effects of the transonic dynamic instability. The corresponding mean total angle-of-attack at drogue chute deployment (see Fig. 12) is 3.6 deg, with a maximum

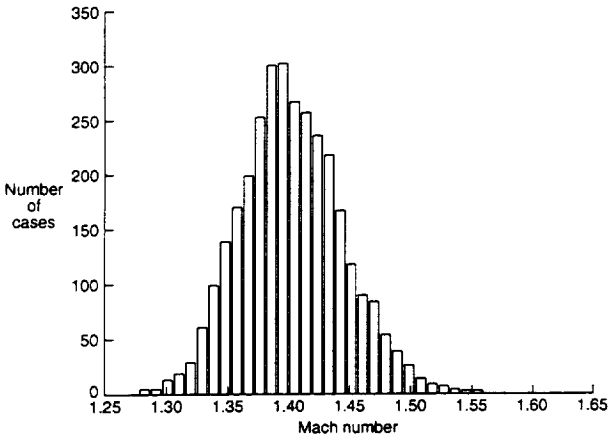

Fig. 11. Distribution of Mach number at drogue chute deployment resulting from over 3200 Monte Carlo simulation cases.

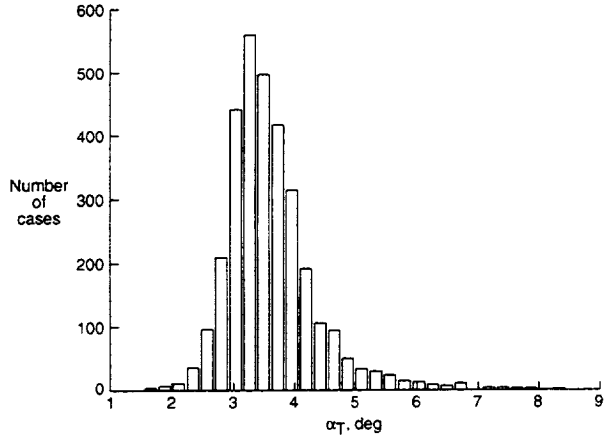

Fig. 12. Distribution of total angle-of-attack at drogue chute deployment resulting from over 3200 Monte Carlo simulation cases.

α_T of 8.4 deg (well below the mission constraint of 30°). Figure 13 shows the distribution of the main parachute deployment altitude. The mean deployment altitude is 3.1 km, with a minimum occurring at 2.21 km.

Figures 14 and 15 show the resulting distributions in downrange and crossrange at landing for the 3200 Monte Carlo cases, respectively. The minimum downrange is -49.4 km (short) from the nominal landing point, whereas the maximum downrange is 54.1 km (long). The maximum crossrange obtained is 18.9 km from the nominal landing point. The resulting 3-σ ellipse has a major axis of 83.5 km (-40.1 short, 42.2 long) in downrange and a minor axis of 29.2 km in crossrange. This footprint is within the UTTR site; however, it is approaching the upper boundary limit. Within the assumptions of

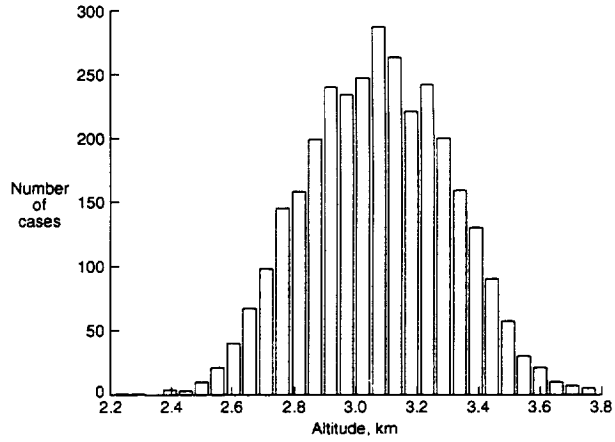

Fig. 13. Distribution of altitude at main chute deployment resulting from over 3200 Monte Carlo simulation cases.

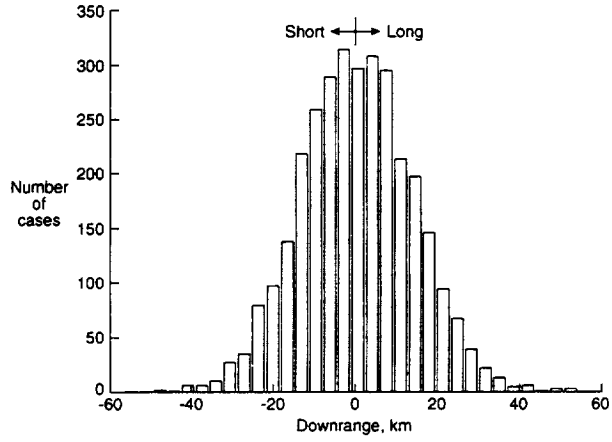

Fig. 14. Downrange distribution at landing resulting from over 3200 Monte Carlo simulation cases.

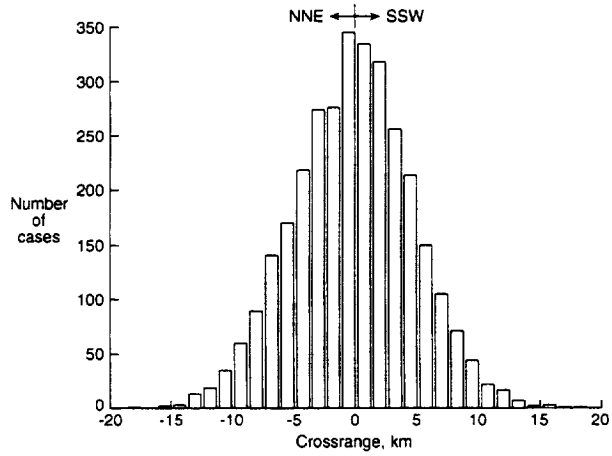

Fig. 15. Crossrange distribution at landing resulting from over 3200 Monte Carlo simulation cases.

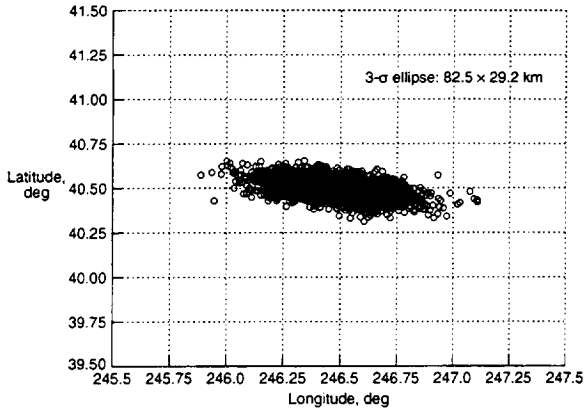

Fig. 16. Landing range dispersion resulting from over 3200 Monte Carlo simulation cases.

Table 5. Summary of Monte-Carlo Analysis

Attitude dispersion	**Mean**	**Min.**	**Max.**	**3-σ**	
Atmospheric interface					
α_T, deg	2.5	0.3	8.0	3.3	
Transitional regime α_T, deg	8.1	1.8	30.4	10.6	
Peak heating α_T, deg	2.5	0.5	8.6	2.5	
Drogue chute deployment					
α_T, deg	3.6	1.5	8.4	2.3	
Landing dispersion					
Landing downrange, km	0.4	-49.4	54.1	42.4	(long)
				-40.1	(short)
Landing crossrange, km	-0.2	-18.7	18.9	14.6	
Total range, km	1.2	0.3	54.5	23.6	

the present analysis, a 99.7 percent probability exists that the SRC will land within this 3-σ footprint ellipse. Figure 16 shows the landing location of all 3200 Monte Carlo cases. Table 5 summaries these results.

SUMMARY

A six-DOF analysis of the nominal Stardust SRC entry reveals that two aerodynamic instabilities result in unacceptable capsule dynamics during the descent. The first instability resides in the high altitude free molecular regime, while the second appears toward the end of the entry in the transonic/subsonic flow regime. These instabilities, if not eliminated or at least suppressed, could lead to mission failure. In the free molecular regime, a static instability exists which produces large excursions in the angle-of-attack (approaching 70°) early in the nominal entry profile. If off-nominal attitudes or attitude rates exist at atmospheric interface, a backward entry is very possible. In the transonic/subsonic regime, a dynamic instability is present which could induce a tumbling motion prior to parachute deployment.

The solution selected to address the high altitude instability is to increase the SRC entry spin rate to 16 rpm. The higher spin rate, although not eliminating the instability, increases the gyroscopic stability of the SRC thereby retarding the effects of the free molecular static instability. To address the transonic/subsonic instability, a drogue chute (having a diameter of 0.828 m) is added and a deployment algorithm based on an accelerometer activated timer resulting in a Mach 1.4 deployment is defined. The drogue chute serves to stabilize the SRC until main parachute deployment, and is shown not to introduce an unacceptably large increase in the landing footprint.

For this mission, 41 potential uncertainties were identified which could impact the entry. Initial state vector and atmospheric property (density, and North-South and East-West winds) uncertainties were found to produce the greatest downrange dispersions on the order of 20-25 km each. Uncertainties from bus separation and aerodynamics produced dispersion between 5-10 km each. All other uncertainties resulted in dispersion less than 1 km.

A Monte Carlo analysis of over 3200 off-nominal trajectories shows that the SRC attitude near peak heating and drogue chute deployment to be within Stardust program limits. The resulting 3-σ landing footprint obtained was 83.5 km (-40.1 short, 42.2 long) in downrange and 29.2 km in crossrange (which is within the Utah Test and Training Range boundaries). Within the assumptions of the present study, a 99.7 percent probability exists that the Stardust SRC will land within this 3-σ ellipse.

The instabilities in the Stardust SRC were revealed too late in the design process. If identified earlier, these types of instabilities could be eliminated by considering alternative capsule configurations that avoid the need for corrective measures later in a program. Therefore, a case is made for including six-DOF entry trajectory analyses early in the conceptual design phase.

Finally, the resolution of the Stardust SRC instabilities relies heavily on the validity of the Monte Carlo analysis more than any previous mission. Increased dependence on entry simulations for mission success places considerable importance on selecting appropriate uncertainties. As confidence increases in the analysis accuracy, cheaper and/or higher performance entry systems can be selected for future missions.

ACKNOWLEDGMENTS

The authors would like to thank Mr. William Willcockson of Lockheed-Martin Astronautics for his contributions in developing the solution to address the instabilities.

REFERENCES

1) Tran, H., Johnson, C., Rasky, D., Hui, F., Chen, Y. K., and Hsu, M., "Phenolic Impregnated Carbon Ablators (PICA) for Discovery Class Missions," AIAA Paper 96-1911, June, 1996.

2) Mitcheltree, R. A., Wilmoth, R. G., Cheatwood, F., M., Brauckmann, G. J., and Greene, F. A., "Aerodynamics of Stardust Sample Return Capsule," AIAA Paper 97-2304, June, 1997.

3) Cheatwood, F. M. and Gnoffo, P. A., "User's Manual for the Langley Aerothermodynamic Upwind Relaxation Algorithm (LAURA)," NASA TM 4674, April 1996.

4) Vatsa, V. N., Turkel, E., Abolhassani, J. S., "Extension of Multigrid Methodology to Supersonic/Hypersonic 3-D Viscous Flows," NASA Contractor Report 187612, Aug. 1991.

5) Mitcheltree, R. A., and Fremaux, C. M., "Subsonic Dynamics of Stardust Sample Return Capsule," NASA TM 110329, March 1997.

6) Brauer, G. L., Cornick, D. E., and Stevenson, R., "Capabilities and Applications of the Program to Optimize Simulated Trajectories (POST)," NASA CR-2770, Feb. 1977.

7) Powell, R. W., and Braun, R. D., "Six-Degree-of-Freedom Guidance and Control Analysis of Mars Aerocapture," *Journal of Guidance, Control, and Dynamics*, Vol. 16, No. 6, 1993, pp. 1038-1044.

8) Braun, R. D., Powell, R. W., Engelund, W. C., Gnoffo, P. A., Weilmuenster, K. J., and Mitcheltree, R. A., "Mars Pathfinder Mission Six-Degree-of-Freedom Entry Analysis," *Journal of Spacecraft and Rockets*, Vol. 32, No. 6, 1995, pp. 993-1000.

9) Desai, P. N., Braun, R. D., Powell, R. W., Engelund, W. C., and Tartabini, P. V., "Six-Degree-of-Freedom Entry Dispersion Analysis for the METEOR Recovery Module," *Journal of Spacecraft and Rockets*, Vol. 34, No. 3, 1997, pp. 334-340.

10) Justus, C. G., Jeffries III, W. R., Yung, S. P., and Johnson, D. L., "The NASA/MSFC Global Reference Atmospheric Model - 1995 Version (GRAM-95)," NASA TM-4715, Aug. 1995.

11) Spencer, D. A., et. al., "Mars Pathfinder Entry, Descent, and Landing Reconstruction," AIAA Paper, AAS/AIAA Space Flight Mechanics Meeting, Monterey, CA , Feb. 1998.

12) Wilmoth, R. G., Mitcheltree, R. A., and Moss, J. N., "Low-Density Aerodynamics of the Stardust Sample Return Capsule," AIAA Paper 97-2510, June 1997.

13) Olynick, D. R., Chen, Y. K., Tauber, M. E., "Forebody TPS Sizing with Radiation and Ablation for the Stardust Sample Return Capsule," AIAA Paper 97-2474, June 1997.